Towards Accurate Prediction for Laser-Coolable Molecules: Relativistic Coupled-Cluster Calculations for Yttrium Monoxide and Prospects for Improving its Laser Cooling Efficiencies

Chaoqun Zhang, 1 Hannah Korslund, 1 Shiqian Ding, $^{2, \, a)}$ and Lan Cheng $^{1, \, b)}$

¹⁾Department of Chemistry, The Johns Hopkins University, Baltimore, MD 21218, USA

²⁾ JILA, National Institute of Standards and Technology and the University of Colorado, Boulder, Colorado 80309-0440, USA and Department of Physics, University of Colorado, Boulder, Colorado 80309-0390, USA

Benchmark relativistic coupled-cluster calculations for yttrium monoxide (YO) with accurate treatment of relativistic and electron correlation effects are reported. The spin-orbit mixing of ${}^{2}\Pi$ and ${}^{2}\Delta$ is found to be an order of magnitude smaller than previously reported in the literature. This together with experimental measurement for the lifetime of the $A'^2\Delta_{3/2}$ state implies an enhanced capability of a narrow-line cooling scheme to bring YO to sub-recoil temperature. The computed electronic transition properties also support a four-photon scheme for closing the leakage of the $A^2\Pi_{1/2} \leftrightarrow X^2\Sigma_{1/2}^+$ cycle through the $A'^2\Delta_{3/2}$ state by repumping the molecules leaking to the $A'^2\Delta_{3/2}$ state to the $B^2\Sigma_{1/2}^+$ state, which subsequently decay back to $X^2\Sigma_{1/2}^+$ states with the same parity as those initially in the optical cycle. Relativistic coupled-cluster methods capable of providing accurate spectroscopic parameters that characterize the local potential curves and hence of providing accurate Franck-Condon factors appear to be promising candidates for accurate predictions of laser-coolable molecules.

a) Electronic mail: Shiqian.ding@colorado.edu

b) Electronic mail: lcheng24@jhu.edu

I. INTRODUCTION

Cold molecules have the potential of providing new avenues for quantum information science, cold chemistry, and precision tests of fundamental physics.^{1–17} Laser cooling techniques offer a promising route for bringing molecules towards the ultracold regime.^{18–25} However, the more complex internal structure of a molecule poses challenges for applying laser-cooling techniques readily established for atoms. A molecule in the vibrational ground state of an electronic upper state can make transitions to a number of vibrational states of a lower electronic state, which requires the use of additional repumping lasers to form nearly closed optical cycles. This leads to complicated molecule-specific experimental setup. The selection of a suitable molecule thus is of importance to the success of an experimental effort. Determination of molecular parameters pertinent to laser cooling mainly relies on experimental measurement using high-resolution laser spectroscopy.^{26–30} At the same time, calculations of these parameters aiming at identifying laser-coolable molecules have also attracted considerable attention.^{31–40}

A class of molecules of particular interest to laser cooling is alkaline or early/late transition metal containing small molecules in their doublet electronic states comprising an alkaline or transition metal atom and an electron-withdrawing ligand. These molecules usually possess an $X^2\Sigma$ ground state with an unpaired electron in the metal s-type orbital. The first manifold of electronically excited states consist of the $A^2\Pi$ and $A'^2\Delta$ states as well as a $B^2\Sigma$ state. Since the unpaired electrons in these excited states are also largely localized at the metal site, these excited states largely preserve the nature of the metal-ligand bond and exhibit geometries and vibrational structures similar to those of the ground state. This

leads to diagonally dominant Franck-Condon factors for transitions between these excited states and the ground state, which is crucial for forming closed optical cycles. Many polar molecules studied in laser cooling fall into this category.^{18–25}

As mentioned above, the most important molecular properties pertinent to laser cooling are perhaps the Franck-Condon factors (FCFs) for transitions between electronic ground and excited states. In particular, FCFs for dipole-allowed $X^2\Sigma \to A^2\Pi$ and $X^2\Sigma \to B^2\Sigma$ transitions as possible candidates for optical cycles are of paramount importance. Pertinent to accurate calculations of FCFs are the local potential energy curves (PECs) around the equilibrium geometries. Therefore, the most important criterion for selecting electronic structure methods is the capability of providing accurate spectroscopic parameters that characterize the local PECs, i.e., the equilibrium structures, harmonic vibrational frequencies, as well as cubic and quartic force constants. Further, the level positions for the $A'^2\Delta$ states and the transition intensities between $A^2\Pi$ and $A'^2\Delta$ are also of significant interest. They are responsible for whether the $X^2\Sigma \leftrightarrow A^2\Pi$ cycle has a significant leakage to the "dark" $A'^2\Delta$ state. Finally, accurate calculation for the spin-orbit mixing between $A'^2\Delta$ and $A^2\Pi$ plays an important role in determining the lifetime and transition properties of the $A'^2\Delta$ states, which is possibly relevant to narrow-line cooling techniques using the $A'^2\Delta$ ${
m state}^{41}$ or repumping schemes to reduce the effects due to leakage of the $A^2\Pi_{1/2}\leftrightarrow X^2\Sigma_{1/2}$ cycle to the $A'^2\Delta_{3/2}$ state.

The present work reports a benchmark computational study of the above mentioned properties pertinent to laser cooling for yttrium monoxide (YO)^{20,42–44} together with prospects for enhancing laser cooling efficiencies for this molecule. Since the prospect schemes use the

 $A'^2\Delta$ state, treatment of spin-orbit effects on the low-lying electronic states of YO, especially on the lifetime and transition properties of the $A'^2\Delta$ state, is one focus of the present study. An experimental measurement of the $A'^2\Delta$ lifetime is also reported here. The implication of $A'^2\Delta - A^2\Pi$ spin-orbit mixing to a narrow-line cooling scheme of YO proposed in Ref.⁴¹ and a new idea of using the $A'^2\Delta_{3/2} \to B^2\Sigma_{1/2}^+$ transition to close the leakage to the $A'^2\Delta_{3/2}$ from the $A^2\Pi_{1/2} \leftrightarrow X^2\Sigma_{1/2}^+$ cycle are discussed. The other focus of the computational study presented here is to use the hierarchies of coupled-cluster methods and systematically expanded basis sets to evaluate the convergence of computational results. A variety of forms for potential energy curves, including ab initio potential, harmonic potential, and Morse potential, have also been used in calculations of Franck-Condon factors to study the effects of the potential function. These analyses as well as comparison with experimental measurements for YO^{45–52} aim to assess the accuracy of computed properties, paving the way to quantitative calculations with predictive value.

II. METHODS

A. Experimental

The experimental measurement reported here focuses on the lifetime of the $A'^2\Delta_{3/2}$ state. A molecular beam at a speed of 100 m/s is generated with a buffer gas cell filled with helium at 4 K temperature. We excite the molecules from $X^2\Sigma_{1/2}^+$ to $A'^2\Delta_{3/2}$ with a resonant laser pulse at 689.6 nm applied perpendicular to the moleculer beam. We then switch off the laser, and collect the fluorescence from the molecules with a photomultiplier tube (PMT). The data is shown in Fig. 1. The measured fluorescence yield is assumed to decay exponentially with respect to time, i.e., $\propto e^{-t/\tau}$ with τ being the lifetime of the $A'^2\Delta_{3/2}$ state, which is extracted

in a fitting procedure to be 23(2) μ s (Fig. 1).

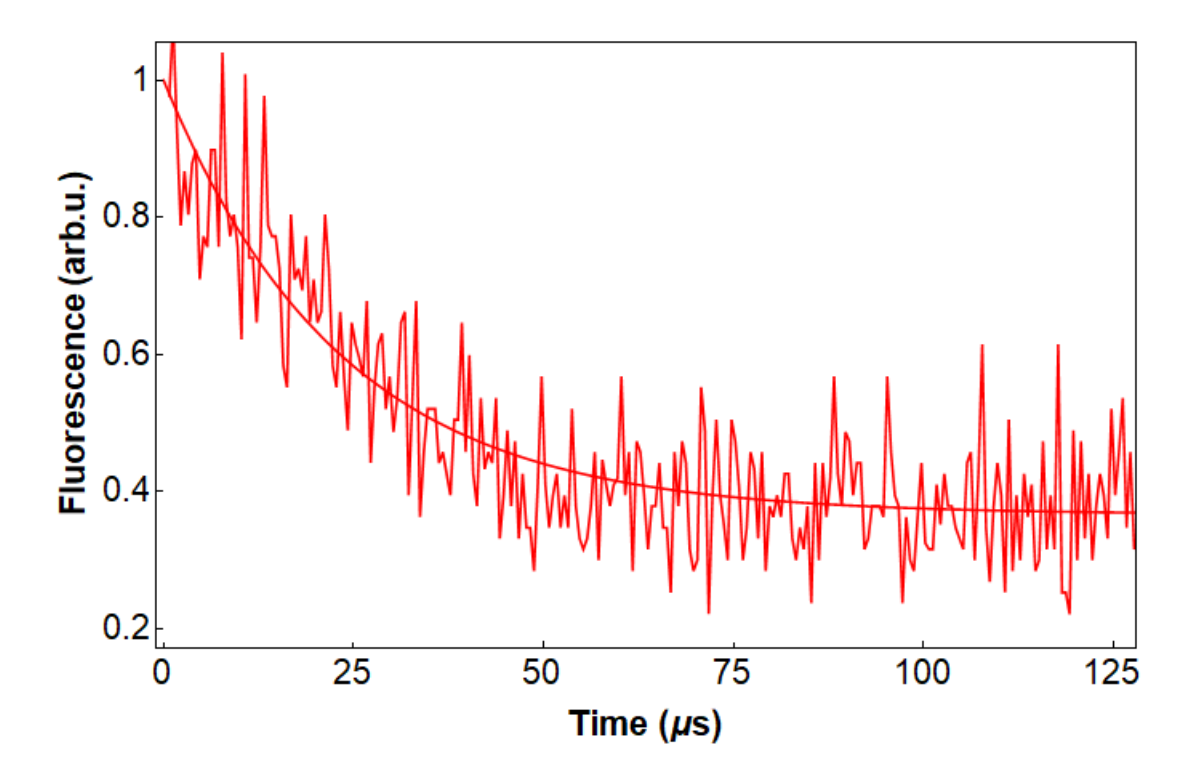


FIG. 1. Measurement of $A'^2\Delta_{3/2}$ lifetime. The jagged line represents the experimental data and the smooth line is a fit to the function $ae^{-t/\tau} + b$.

B. Computational

The CFOUR program package^{53–59} has been used in all computations presented here. The electron configurations of the $X^2\Sigma^+$, $A^2\Pi$, $A'^2\Delta$, and $B^2\Sigma^+$ states of YO comprise the same closed-shell cationic configuration augmented with an additional unpaired electron occupying the valence 1σ , 1π , 1δ , and 2σ orbitals, respectively. Since the closed-shell configuration is stable, response theories using the closed-shell configuration as the reference and adding one electron to obtain the target states, e.g., the equation-of-motion electron attachment coupled cluster (EOMEA-CC)⁶⁰ methods, are expected to provide balanced descriptions for

these states. To investigate the accuracy of EOMEA-CC methods for the present application, we have carried out EOMEA-CC singles and doubles (CCSD) and singles doubles triples (CCSDT) calculations for the equilibrium geometries and vibrational frequencies of these four electronic states of YO. The EOMEA-CCSDT calculations have used the recent efficient implementation of EOM-CCSDT for excitation energies within the CFOUR program⁶¹ together with the continuum-orbital trick⁶² for accessing electron attached states. The scalar-relativistic effects have been taken into account using the spin-free exact twocomponent theory in its one-electron variant (SFX2C-1e)^{57,63,64} unless otherwise specified. Perturbative treatment of spin-orbit coupling has been performed using spin-orbit integrals of the SFX2C-1e atomic mean-field (AMF) spin-orbit approach⁶⁵ and spin-orbit coupling matrix elements computed using the EOM-CCSD expectation-value formulation, ^{66,67} hereby taking the SFX2C-1e wavefunctions as the zeroth-order wavefunctions⁶⁸. In this way, scalarrelativistic contributions to both the unperturbed states and the spin-orbit integrals have been taken into account. This perturbative scheme has recently been shown to provide accurate spectroscopic parameters for the ThO⁺ molecule, ⁶⁵ which has an electronic structure similar to YO.

Unrestricted Hartree-Fock (UHF) based coupled-cluster singles doubles augmented with a noniterative triples $[CCSD(T)]^{69,70}$ calculations have also been performed for the $X^2\Sigma^+$, $A^2\Pi$, and $A'^2\Delta$ states, which are the lowest electronic states in the corresponding irreducible representations. We have also carried out CCSD(T) calculations with non-perturbative treatment of spin-orbit coupling $[SO-CCSD(T)]^{71}$ using the X2C scheme^{64,72,73} and the corresponding AMF approach⁷⁴ for the $X^2\Sigma^+_{1/2}$, $A'^2\Delta_{3/2}$, and $A'^2\Delta_{5/2}$ states to obtain benchmark results for treatment of both spin-orbit coupling and electron correlation. These

CCSD(T) calculations directly optimize the wavefunctions for the targeted states, and thus are expected to provide more accurate energies and properties than EOM-CC calculations when a similar level of truncation for the cluster expansion is applied. On the other hand, it should be noted that the EOM-CC methods are more flexible than the UHF-CC methods, especially for states that are not the lowest in an irreducible representation. Although we have converged UHF-CCSD(T) calculations for the $B^2\Sigma^+$ state as well as SO-CCSD(T) calculations for the $A^2\Pi_{1/2}$ and $A^2\Pi_{3/2}$ states in the vicinity of the equilibrium structures by using a maximum-overlap method (MOM),⁷⁵ convergence difficulties have been encountered for SO-CCSD(T) calculations of the $B^2\Sigma_{1/2}^+$ state.

The contraction coefficients of standard basis sets have been constructed for scalar-relativistic calculations. In the present study, we have used basis sets in the fully uncontracted form to ensure sufficient degrees of freedom for accurately accounting for both scalar-relativistic and spin-orbit effects. The set of primitive s-, p-, d- functions of the ANO-RCC basis set for yttrium⁷⁶ are augmented with correlating functions of cc-pCVTZ and cc-pCVQZ basis sets⁷⁷ to form TZ and QZ sets for yttrium. The uncontracted correlation consistent cc-pCVTZ and cc-pCVQZ basis sets of oxygen have been used and are denoted as TZ and QZ sets for oxygen.⁷⁸ Virtual orbitals with orbital energies greater than 1000 hartree have been kept frozen in all CC calculations.

For each scheme of electronic-structure calculations, the local potential energy curves (PECs) have been scanned and fitted into sixth-order polynomial functions. Equilibrium bond lengths, harmonic vibrational frequencies, and anharmonic constants were obtained using these force constants and second-order vibrational perturbation theory.⁷⁹ More exten-

sive calculations of PECs in the range of bond lengths [1.55 Å, 2.20 Å] covering around 10000 cm⁻¹ above the energies of the equilibrium geometries have also been performed for EOM-CC calculations. These computed energies have been fitted into tenth-order polynomials to reproduce the energies in this region faithfully. These ab initio PECs (documented in the supplementary material) have been used for discrete variable representation (DVR) calculations to obtain vibrational wavefunctions, energy levels, and Franck-Condon factors. DVR calculations have also been carried out using harmonic and Morse potentials with spectroscopic parameters including bond lengths, harmonic frequencies, and anharmonic constants obtained from ab initio calculations or experiments to test how the forms of PECs affect the computed Franck-Condon factors.

III. RESULTS AND DISCUSSIONS

A. Spin-orbit mixing and electronic transition dipole moments

The compositions of the $X^2\Sigma_{1/2}^+$, $A^2\Pi_{1/2}$, $A^2\Pi_{3/2}$, $A'^2\Delta_{3/2}$, $A'^2\Delta_{5/2}$, and $B^2\Sigma_{1/2}^+$ wavefunctions in terms of scalar-relativistic wavefunctions in the bond length of 1.8 Å have been obtained by diagonalizing the effective Hamiltonian (Table I) and summarized in Table II. The spin-orbit mixing between these scalar-relativistic wavefunctions is in general small, e.g., the $A'^2\Delta_{3/2}$ state has a contribution of less than 0.1% from the $^2\Pi$ wavefunction (an expansion coefficient of ca. 0.03). Importantly, the $^2\Pi - ^2\Delta$ spin-orbit mixing obtained in the present calculations is substantially smaller than the value reported in Ref. ⁴⁸ calculated using the spin-orbit coupling strength of yttrium 4d orbitals. This discrepancy can be attributed to that the $^2\pi$ orbitals are dominated by yttrium 5 p±1 contributions with only small contributions from 4 d±1 orbitals (Figure 1). Note that yttrium atomic spin-orbit

interaction directly couples $4d_{\pm 2}$ with $4d_{\pm 1}$ but not with $5p_{\pm 1}$. Therefore, as shown in Table I, the spin-orbit matrix elements between the $^2\Pi$ and $^2\Delta$ wavefunctions amount to less than $30~{\rm cm}^{-1}$, one order of magnitude smaller than those between $^2\Delta_{xz}$ and $^2\Delta_{yz}$ wavefunctions. The small $^2\Pi$ and $^2\Delta$ spin-orbit mixing has important implications for the lifetime of the $A'^2\Delta$ state and the transition intensities of nominally dipole forbidden $A'^2\Delta \leftrightarrow X^2\Sigma$ and $A'^2\Delta \leftrightarrow B^2\Sigma$ transitions, as detailed below.

Computed electronic transition dipole moments between scalar-relativistic wavefunctions as summarized in Table III compare reasonably well with computational results reported in Ref. 80. The transition dipole moments for dipole-allowed transitions between spin-orbit-coupled stated including the $X^2\Sigma_{1/2}^+ \leftrightarrow A^2\Pi_{1/2}$, $X^2\Sigma_{1/2}^+ \leftrightarrow B^2\Sigma_{1/2}^+$, and $A^2\Pi_{1/2} \leftrightarrow A'^2\Delta_{3/2}$ transitions largely derive from the corresponding values between scalar-relativistic wavefunctions. The lifetime values of 26 ns and 24 ns for the $A^2\Pi_{1/2}$ and $A^2\Pi_{3/2}$ states obtained using the Einstein A coefficients in Table IV compare favorably with experimental values of 33 ns and 30ns. 46 The computed lifetime of ca. 20 ns for the $B^2\Sigma_{1/2}^+$ state is similar to those of the $A^2\Pi$ states. The transition moment for the $A^2\Pi_{1/2} \leftrightarrow A'^2\Delta_{3/2}$ transition is of similar magnitude to that of the $X^2\Sigma_{1/2}^+ \leftrightarrow B^2\Sigma_{1/2}^+$ transition. Owing to the much smaller transition energy, the spontaneous decay rate from $A^2\Pi_{1/2}$ to $A'^2\Delta_{3/2}$ is three orders of magnitude lower than that from $A^2\Pi_{1/2}$ to $X^2\Sigma_{1/2}^+$. The computed branching ratio of 6×10^{-4} for $A^2\Pi_{1/2} \to A'^2\Delta_{3/2}$ is in reasonable agreement with the value of 3×10^{-4} reported in Ref. 41

The $X^2\Sigma_{1/2}^+\leftrightarrow A'^2\Delta_{3/2}$ and $A'^2\Delta_{3/2}\leftrightarrow B^2\Sigma_{1/2}^+$ transitions are nominally dipole forbidden and borrow intensities entirely through spin-orbit mixing. As shown in Table IV, the transition moment for the $X^2\Sigma_{1/2}^+\leftrightarrow A'^2\Delta_{3/2}$ transition is three order of magnitude smaller

than that of the dipole-allowed $X^2\Sigma_{1/2}^+ \leftrightarrow A^2\Pi_{1/2}$ transition. This leads to a value of 40 μ s for the spontaneous decay lifetime of the $A'^2\Delta_{3/2}$ state, around 1500 times longer than that of the $A^2\Pi_{1/2}$ state. This computed lifetime for the $A'^2\Delta_{3/2}$ state is in good agreement with the measured value of 23(2) μ s presented in Section II-A. The $A'^2\Delta_{3/2} \leftrightarrow B^2\Sigma_{1/2}^+$ transition has an oscillator strength of similar magnitude to that of the $X^2\Sigma_{1/2}^+ \leftrightarrow A'^2\Delta_{3/2}$ transition. Finally, since the unpaired electrons in the $X^2\Sigma^+$, $A^2\Pi$, and $B^2\Sigma^+$ states are dominated by yttrium 5s, $5p_x/5p_y$, and $5p_z$ orbitals, respectively, $B^2\Sigma_{1/2}^+ \leftrightarrow A^2\Pi_{1/2}$ transition possesses a much smaller transition dipole moment (25 times smaller) than that of the $X^2\Sigma_{1/2}^+ \leftrightarrow B^2\Sigma_{1/2}^+$ transition. Consequently, the oscillator strength of this transition is only about the same magnitude as those of dipole-forbidden transitions.

B. Benchmark calculations of molecular parameters and Franck-Condon factors

1. Equilibrium geometries, harmonic frequencies, and term energies

Since Franck-Condon factors (FCFs) involving low-lying vibrational states are largely determined by the local potential energy curves (PECs), we first focus on structural parameters such as equilibrium bond lengths and vibrational frequencies that characterize the local PECs. In general, EOM-CCSD provides qualitatively correct results, while the inclusion of triples contributions build the way to obtain accurate results. The triples corrections (the difference between EOM-CCSDT and EOM-CCSD, the first two columns in Tables V and VI) amount to around 0.02 Å for equilibrium bond lengths and around 50 cm⁻¹ for harmonic frequencies. EOM-CCSD underestimates the bond lengths and overestimate harmonic frequencies for all the electronic states studied here. The basis-set and

core-correlation effects are smaller, i.e., around 0.005 Å for the bond lengths and a few cm⁻¹ for harmonic frequencies. Spin-orbit corrections (the difference between the fourth and fifth columns in Tables V and VI) amount to around 0.001 Å for bond lengths and a few cm⁻¹ for harmonic frequencies. The deviations between the best EOM-CC results (the columns "EOM-CCSD/ ∞ Z/sc+ Δ T+ Δ SO" in Tables V and VI) and experimental values are below 0.005 Å for bond lengths and 15 cm⁻¹ for harmonic frequencies.

As shown in Tables V and VI, SO-CCSD(T) bond lengths are as accurate as the best EOM values, while SO-CCSD(T) harmonic frequencies agree with experiment even more closely. Namely, SO-CCSD(T) harmonic frequencies are around 5 cm⁻¹ higher than the corresponding experimental values, while the EOM values are 10 cm⁻¹ lower than the experiments. A notable exception is that, although it is also 15 cm⁻¹ higher than the EOM values, CCSD(T) harmonic frequency for $B^2\Sigma^+$ is more than 20 cm⁻¹ greater than the experimental value. This might be due to a perturbing electronic state nearly degenerate to vibrational excited states of $B^2\Sigma^{+51}$ and seems worth further investigation. The perturbing electronic state is not expected to have significant effects on the present calculations of Franck-Condon factors, which only include vibrational ground state of $B^2\Sigma^+$. Note that CCSD(T) features a noniterative triples correction to CCSD with a cost of a single step that scales as the seventh power of the system size, while the cost of CCSDT scales as the eighth power of the system size for each CC iteration. Therefore, CCSD(T) appears to be a more efficient approach for the present purpose of obtaining accurate spectroscopic parameters for YO. The SO effects obtained from SO-CCSD(T) calculations are consistent with those obtained from perturbative SO calculations, e.g., the spin-orbit splittings of bond lengths and harmonic frequencies amount to around 0.001 Å and 1 cm-1.

Unlike in calculations of bond lengths and harmonic frequencies, basis-set effects play an important role in calculations of term energies. Since the $X^2\Sigma$ and $A'^2\Delta$ states possess quite different electronic orbital angular momenta, differential basis-set effects on the term energy of $A'^2\Delta$ are significant. As shown in Table VII, the remaining basis-set effects for the term energies of the $A^{\prime 2}\Delta$ states obtained using the TZ basis amount to more than 600 cm⁻¹. It thus is necessary to perform basis-set extrapolation⁸¹ to estimate the basis-set-limit values to obtain accurate results. CCSD(T) appear to be more accurate than EOM-CCSDT for term energies, e.g., EOM-CCSDT term energies of the $A'^2\Delta$ states appear to be 200 cm⁻¹ too high, while the SO-CCSD(T) ones agree with the experimental values to within 50 ${\rm cm^{-1}}$. Perturbative spin-orbit calculations have obtained values of 285 ${\rm cm^{-1}}$ and 423 ${\rm cm^{-1}}$ for the spin-orbit splittings of the $A'^2\Delta$ and $A^2\Pi$ states, which compare reasonably well with experimental values of 339 cm⁻¹ and 431 cm⁻¹. SO-CCSD(T) provides more accurate spin-orbit splittings, which agree with experimental values to within 5 cm⁻¹. Computed term energies are obviously less accurate than experimental values obtained from using high resolution laser spectroscopy. On the other hand, for electronic states in absence of experimental measurements, e.g., the $A^{\prime 2}\Delta$ state of BaF or RaF, one may speculate that electronic-structure calculations may provide useful estimate for energy levels to facilitate experimental search for these states.

2. Franck-Condon factors

As vibrational overlap integrals, Franck-Condon factors (FCFs) are expected to be sensitive to the difference between the equilibrium bond lengths of two electronic states. The variation of computed FCFs with respect to bond-length differences is demonstrated in

Table VIII with calculations using the same PECs with shifted equilibrium bond lengths. The absolute values of individual FCFs are very sensitive to the variation of bond-length differences, with an approximate linear dependence. For example, a shift of the bond-length difference by 0.005 (or 0.01) Å leads to a change of the FCF for the $B^2\Sigma(0) \to X^2\Sigma(0)$ transition by around 5% (or 10%). On the other hand, the sum of FCFs up to a certain vibrational level is less sensitive to the change of bond-length difference. For example, the sum of FCFs for the $B^2\Sigma^+(0) \to X^2\Sigma^+(v)$ transitions with v = 0 - 3 (v = 0 - 4) saturates to 99.99% (99.999%) for all calculations with a shift of bond-length difference less than 0.01 Å. In general it seems necessary to have bond-length difference accurate to within 0.01 Å to obtain qualitatively correct results for FCFs and to within 0.003 Å to obtain quantitative results. We mention that, as show in supplementary material, the dependence of computed FCFs with respect to harmonic frequencies is less pronounced.

As discussed in the previous section, the EOM-CCSD equilibrium bond lengths differ from experimental values by more than 0.01 Å. One may expect significant errors in computed bond-length differences and FCFs. However, it should be noted that EOM-CCSD consistently overestimates the equilibrium bond lengths for all electronic states studied here; the errors for EOM-CCSD bond-length differences thus are less than 0.01 Å. Consequently, while EOM-CCSD tends to overestimate the diagonal FCFs, EOM-CCSD results are in general robust and qualitatively correct. As shown in Table IX, the deviations of the EOM-CCSD result from those of EOM-CCSDT amount to 1% for the FCF of the $B^2\Sigma^+(0) \to X^2\Sigma^+(0)$ transition and to 4% for the FCF of the $A'^2\Delta(0) \to X^2\Sigma^+(0)$ transition. The vibrational transitions required to saturate the sum of $A^2\Pi(0) \to X^2\Sigma^+(\nu)$ FCFs to more than 99.999% are both $\nu = 0 - 2$ for EOM-CCSD and EOM-CCSDT calculations.

We mention that enlargement of basis sets reduces the bond lengths for all electronic states and has small effects on bond-length differences and hence FCFs (shown as the differences between the second and third columns of Table IX). The effects of core correlation and spin-orbit coupling appear to be even smaller.

The forms of the potential energy functions seem to play a minor role in calculations of FCFs. While the use of harmonic approximation could introduce significant errors for transitions to higher vibrational levels (see the difference between the first and second columns of Table X), the results obtained using Morse potentials agree closely with those obtained using ab initio potentials, provided they share the same equilibrium bond lengths, harmonic frequencies, and anharmonic constants. The first and third columns of Table X respectively show FCFs obtained using the best EOM potential and the Morse potential with the same spectroscopic parameters. The differences between these FCFs are essentially negligible. In contrast, the results obtained using EOM and experimental parameters (columns 3 and 4 in Table X) differ more substantially. When the EOM potential is shifted to match the experimental equilibrium bond length (the last column of Table X), the results agree very well with those obtained using Morse potentials with experimental parameters. Since the semiempirical Morse potentials with accurate spectroscopic parameters are capable of providing accurate FCFs, a useful practical computational strategy is to obtain spectroscopic parameters from relativistic CCSD(T) or EOM-CC calculations and then calculate FCFs using Morse potentials built with these parameters.

C. Prospects for enhancing laser cooling efficiencies for YO

1. An alternative scheme for addressing the leakage through the $^2\Delta_{3/2}$ state

A typical experiment to laser cool molecules requires scattering $\sim 10^5$ photons. The YO molecules with an initial speed of 100 m/s are first slowed to ~ 5 m/s⁴², and then captured by a magneto-optical trap⁴³ and laser cooled to 4 μ K⁸². The transition $X^2\Sigma^+ \leftrightarrow A^2\Pi_{1/2}$ forms an optical cycling transition. Only two vibrational repumpers are required to scatter enough number of photons (to obtain an optical cycle with branching ratios saturated to >99.999%), which is consistent with the present computational results for FCFs in Table X. However, except decaying to $X^2\Sigma^+$, YO molecules also leak to $A'^2\Delta_{3/2}$ from $A^2\Pi_{1/2}$ with a branching ratio on the order of 10^{-4} (6×10^{-4} as derived from Table IV and 3×10^{-4} as reported in Ref.⁴²). The molecules in the $A'^2\Delta_{3/2}$ state subsequently decays to the $X^2\Sigma_{1/2}^+$ state. The optical cycle involving the leakage to $A'^2\Delta_{3/2}$ is a three-photon process, which leads to a decay to the molecular states with the opposite parity compared with the initial state. Separate lasers or microwaves are required to repump these dark states in various rotational states back to the initial states, as demonstrated in Ref. 42,43. However, the FCFs of the $X^2\Sigma_{1/2} \leftrightarrow {}^2\Delta_{3/2}$ transition are not highly diagonal with the FCF of the $X^2\Sigma_{1/2}^+(0) \leftrightarrow {}^2\Delta_{3/2}(0)$ transition being less than 90% (Table X). More than one vibrational states may possibly need to be repumped to enable scattering of 10⁵ photons, which substantially complicates the repumping scheme.

We present here an alternative scheme to close the leakage through $A'^2\Delta_{3/2}$ by coupling $A'^2\Delta_{3/2}$ to $B^2\Sigma_{1/2}^+$. The formally dipole-forbidden transition $A'^2\Delta_{3/2} \leftrightarrow B^2\Sigma_{1/2}^+$ borrows intensity from spin-orbit coupling and has a similar oscillator strength as $X^2\Sigma_{1/2}^+ \leftrightarrow A'^2\Delta_{3/2}$

(Table IV). It is therefore feasible to fully saturate this transition using a laser at 1.602 μ m with a saturation intensity of 0.19 μ W/cm². This reduces the probability for $A'^2\Delta_{3/2}$ to spontaneously decay to $X^2\Sigma_{1/2}$ by a factor of $\tau_{A'}/\tau_B \sim 10^3$, where $\tau_{A'}$ and τ_B are the lifetimes of $^2\Delta_{3/2}$ and $B^2\Sigma_{1/2}^+$, respectively, since $B^2\Sigma_{1/2}^+$ decays much faster than $A'^2\Delta_{3/2}$. This suppression factor is high enough for us to ignore the direct decay from $A'^2\Delta_{3/2}$. The molecules in the $B^2\Sigma^+$ state subsequently decay to the $A^2\Pi_{1/2}$ and $X^2\Sigma_{1/2}^+$ states. Note that the $B^2\Sigma_{1/2}^+ \leftrightarrow A^2\Pi_{1/2}$ transition possesses a very small transition dipole moment, 25 times smaller than that of the $B^2\Sigma_{1/2}^+ \leftrightarrow X^2\Sigma_{1/2}^+$ transition (Table IV). Consequently, the spontaneous decay rate of the former transition is four orders of magnitude smaller than that of the latter one. This indicates that a vast majority of the molecules in the $B^2\Sigma_{1/2}^+$ state decay directly to the ground electronic state. This optical cycle involves $X^2\Sigma_{1/2}^+$, $A^2\Pi_{1/2}$, $A'^2\Delta_{3/2}$, and $B^2\Sigma_{1/2}^+$ states and is a four-photon process with the parity of the states conserved. Therefore, the molecules decay back to the same rotational states as those of $X^2\Sigma_{1/2}^+$ initially in the $X^2\Sigma^+ \leftrightarrow A^2\Pi_{1/2}$ optical cycle.

2. Narrow-line cooling below recoil temperature

A narrow-line cooling scheme using the narrow linewidth of the $A'^2\Delta_{3/2}$ state has been proposed and analyzed in detail in Ref.⁴¹. Since the $^2\Delta_{-2}\Pi$ spin-orbit mixing is significantly lower than previously reported, the linewidth of the $A'^2\Delta_{3/2}$ state is much narrower than that used in Ref.⁴¹. It would thus be of interest to update the analysis for the narrow-line cooling scheme. The Doppler temperature estimated using the measured lifetime of 23 μ s for the $A'^2\Delta_{3/2}$ state is as low as 160 nK, which is comparable with the recoil temperature of ca. 200 nK and more than one order of magnitude lower than the lowest temperature achieved so far for laser-cooled molecules. We mention that the Doppler temperature es-

timated using the computed lifetime of 40 μ s amounts to around 100 nK. Here we adopt the more conservative value of 160 nK in our discussion. This deep cooling can be applied following the gray molasses cooling, which is recently shown to be able to cool YO molecules to 4 μ K. According to the computed FCFs of the $X^2\Sigma_{1/2}^+ \leftrightarrow A'^2\Delta_{3/2}$ transition (the last two columns of Table X), repumping one vibrationally excited state forms an optical cycle containing around 99% vibrational branching. This enables \sim 100 photon scatterings and might be enough for sub-recoil cooling.

The linewidth of $^2\Delta_{3/2}$ is appropriate for employing the SWAP^{83–85} cooling to YO molecules⁸⁶. This technique has been recently demonstrated for Sr atoms^{83,85} using a transition with a similar linewidth. It relies on the time-ordered photon absorption and emission, and substantially reduces the required number of photon scattering events. It opens up the possibility for laser cooling a large class of molecules with less diagonal FCFs.

It has been proposed to implement quantum gates with diatomic molecules by making use of the dipole-dipole interaction^{87,88}. The rapid progress in creating ultracold molecules, either by association of ultracold atoms or by direct laser cooling of molecules, and loading them in an optical lattice⁸⁹ or an optical tweezer array⁹⁰ make this perspective particularly appealing. Control of the molecular motion in the quantum regime is desirable for high gate fidelity⁸⁸. However, due to the large tensor Stark shifts presented in molecules, it is challenging to apply the cooling techniques demonstrated for atoms, e.g., Raman sideband cooling, to molecules⁹¹. This challenge can be overcome by using the narrow-line cooling, as demonstrated in alkaline earth atoms^{92–95}. It represents a simple method to control the molecular motion in the quantum regime, which paves the way for implementing quantum gates between dipolar molecules in optical tweezers.

IV. SUMMARY AND OUTLOOK

Benchmark calculations for the electronic and vibrational structures of low-lying electronic states of YO are reported. Coupled-cluster methods, which offer accurate treatment of electron correlation around equilibrium structures, appear to be promising candidates for accurate calculations of Franck-Condon factors. In this context, accurate calculation of equilibrium structures seems of paramount importance. It would be of particular interest to extend the coupled-cluster techniques for obtaining highly accurate structures for molecules containing light elements^{96,97} to heavy-metal containing molecules by including scalar-relativistic and spin-orbit effects.

A four-photon process comprising repumping from the $A'^2\Delta_{3/2}$ state to the $B^2\Sigma_{1/2}^+$ state is proposed to address leakage of the $A^2\Pi_{1/2} \leftrightarrow X^2\Sigma_{1/2}^+$ cycle through the $A'^2\Delta_{3/2}$ state and enhance the efficiency for laser cooling YO. This scheme is supported by the computed electronic transition properties and Franck-Condon factors presented in this work. Further, prospects of a narrow-line cooling scheme⁴¹ using the $A'^2\Delta_{3/2}$ state have been updated using the computed transition properties and measured lifetime of the $A'^2\Delta_{3/2}$ state. This narrow-line cooling scheme seems to have the potential of bringing YO to sub-recoil temperature.

V. ACKNOWLEDGEMENT

The work at Johns Hopkins University was supported by the National Science Foundation, under grant No. PHY-1011794. S. D. is indebted to Jun Ye (Boulder) for his generous support. L. C. would like to thank Jinjun Liu (Louisville) for stimulating discussions. All computations have been performed at the Maryland Advanced Research Computing Center.

REFERENCES

- ¹L. D. Carr, D. DeMille, R. V. Krems, and J. Ye, New J. Phys. **11**, 55049 (2009).
- ²L. R. Liu, J. D. Hood, Y. Yu, J. T. Zhang, N. R. Hutzler, T. Rosenband, and K.-K. Ni, Science (80-.). **360**, 900 LP (2018).
- ³L. Anderegg, L. W. Cheuk, Y. Bao, S. Burchesky, W. Ketterle, K.-K. Ni, and J. M. Doyle, Science (80-.). **365**, 1156 LP (2019).
- ⁴M. T. Bell and T. P. Softley, Mol. Phys. **107**, 99 (2009).
- ⁵S. Ospelkaus, K.-K. Ni, D. Wang, M. H. G. de Miranda, B. Neyenhuis, G. Quéméner, P. S. Julienne, J. L. Bohn, D. S. Jin, and J. Ye, Science (80-.). **327**, 853 LP (2010).
- ⁶J. M. Hutson, Science (80-.). **327**, 788 LP (2010).
- ⁷G. Quéméner and P. S. Julienne, Chem. Rev. **112**, 4949 (2012).
- ⁸K.-K. Ni, S. Ospelkaus, M. H. G. de Miranda, A. Pe'er, B. Neyenhuis, J. J. Zirbel,
 S. Kotochigova, P. S. Julienne, D. S. Jin, and J. Ye, Science (80-.). 322, 231 LP (2008).
 ⁹J. J. Hudson, B. E. Sauer, M. R. Tarbutt, and E. A. Hinds, Phys. Rev. Lett. 89, 23003 (2002).
- 10 E. R. Meyer, J. L. Bohn, and M. P. Deskevich, Phys. Rev. A 73, 62108 (2006).
- ¹¹H. Loh, K. C. Cossel, M. C. Grau, K.-K. Ni, E. R. Meyer, J. L. Bohn, J. Ye, and E. A. Cornell, Science (80-.). 342, 1220 LP (2013).
- ¹²J. and Baron, W. C. Campbell, D. DeMille, J. M. Doyle, G. Gabrielse, Y. V. Gurevich, P. W. Hess, N. R. Hutzler, E. Kirilov, I. Kozyryev, B. R. O'Leary, C. D. Panda, M. F. Parsons, E. S. Petrik, B. Spaun, A. C. Vutha, and A. D. West, Science (80-.). 343, 269 LP (2014).

- ¹³V. Andreev, D. G. Ang, D. DeMille, J. M. Doyle, G. Gabrielse, J. Haefner, N. R. Hutzler, Z. Lasner, C. Meisenhelder, B. R. O'Leary, C. D. Panda, A. D. West, E. P. West, X. Wu, and A. Collaboration, Nature 562, 355 (2018).
- ¹⁴W. B. Cairncross, D. N. Gresh, M. Grau, K. C. Cossel, T. S. Roussy, Y. Ni, Y. Zhou, J. Ye, and E. A. Cornell, Phys. Rev. Lett. **119**, 153001 (2017).
- $^{15}\mathrm{I}.$ Kozyryev and N. R. Hutzler, Phys. Rev. Lett. $\mathbf{119},\,133002$ (2017).
- ¹⁶D. DeMille, J. M. Doyle, and A. O. Sushkov, Science (80-.). **357**, 990 LP (2017).
- $^{17}\mathrm{W}.$ B. Cairncross and J. Ye, Nat. Rev. Phys. 1, 510 (2019).
- ¹⁸J. D. Weinstein, R. DeCarvalho, T. Guillet, B. Friedrich, and J. M. Doyle, Nature 395, 148 (1998).
- ¹⁹E. S. Shuman, J. F. Barry, and D. DeMille, Nature **467**, 820 (2010).
- ²⁰M. T. Hummon, M. Yeo, B. K. Stuhl, A. L. Collopy, Y. Xia, and J. Ye, Phys. Rev. Lett. 110, 143001 (2013).
- ²¹I. Kozyryev, L. Baum, K. Matsuda, and J. M. Doyle, ChemPhysChem 17, 3641 (2016).
- ²²I. Kozyryev, L. Baum, K. Matsuda, B. L. Augenbraun, L. Anderegg, A. P. Sedlack, and J. M. Doyle, Phys. Rev. Lett. 118, 173201 (2017).
- ²³S. Truppe, H. J. Williams, M. Hambach, L. Caldwell, N. J. Fitch, E. A. Hinds, B. E. Sauer, and M. R. Tarbutt, Nat. Phys. 13, 1173 (2017).
- ²⁴L. Anderegg, B. L. Augenbraun, Y. Bao, S. Burchesky, L. W. Cheuk, W. Ketterle, and J. M. Doyle, Nat. Phys. 14, 890 (2018).
- ²⁵J. Lim, J. R. Almond, M. A. Trigatzis, J. A. Devlin, N. J. Fitch, B. E. Sauer, M. R. Tarbutt, and E. A. Hinds, Phys. Rev. Lett. **120**, 123201 (2018).
- ²⁶I. Kozyryev, T. C. Steimle, P. Yu, D.-T. Nguyen, and J. M. Doyle, New J. Phys. **21**, 52002 (2019).

- ²⁷E. T. Mengesha, A. T. Le, T. C. Steimle, L. Cheng, C. Zhang, B. L. Augenbraun, Z. Lasner, and J. Doyle, J. Phys. Chem. A **124**, 3135 (2020).
- ²⁸X. Zhuang, A. Le, T. C. Steimle, N. E. Bulleid, I. J. Smallman, R. J. Hendricks, S. M. Skoff, J. J. Hudson, B. E. Sauer, E. A. Hinds, and M. R. Tarbutt, Phys. Chem. Chem. Phys. 13, 19013 (2011).
- ²⁹D.-T. Nguyen, T. C. Steimle, I. Kozyryev, M. Huang, and A. B. McCoy, J. Mol. Spectrosc. **347**, 7 (2018).
- ³⁰A. C. Paul, K. Sharma, M. A. Reza, H. Telfah, T. A. Miller, and J. Liu, J. Chem. Phys. 151, 134303 (2019).
- ³¹B. Rafei, G. Younes, and M. Korek, J. Phys. Conf. Ser. **869**, 12001 (2017).
- ³²Q.-Q. Zhang, C.-L. Yang, M.-S. Wang, X.-G. Ma, and W.-W. Liu, J. Phys. B At. Mol. Opt. Phys. 51, 155102 (2018).
- ³³J. Cui, J.-G. Xu, J.-X. Qi, G. Dou, and Y.-G. Zhang, Chinese Phys. B **27**, 103101 (2018).
- ³⁴I. Zeid, T. Atallah, S. Kontar, W. Chmaisani, N. El-Kork, and M. Korek, Comput. Theor. Chem. 1126, 16 (2018).
- ³⁵C. Li, Y. Li, Z. Ji, X. Qiu, Y. Lai, J. Wei, Y. Zhao, L. Deng, Y. Chen, and J. Liu, Phys. Rev. A 97, 62501 (2018).
- ³⁶Y. Hao, L. F. Pašteka, L. Visscher, P. Aggarwal, H. L. Bethlem, A. Boeschoten, A. Borschevsky, M. Denis, K. Esajas, S. Hoekstra, K. Jungmann, V. R. Marshall, T. B. Meijknecht, M. C. Mooij, R. G. E. Timmermans, A. Touwen, W. Ubachs, L. Willmann, Y. Yin, and A. Zapara, J. Chem. Phys. 151, 34302 (2019).
- ³⁷M. V. Ivanov, F. H. Bangerter, and A. I. Krylov, Phys. Chem. Chem. Phys. **21**, 19447 (2019).

- ³⁸H. Ladjimi, W. Zrafi, A.-R. Allouche, and H. Berriche, J. Quant. Spectrosc. Radiat. Transf. **252**, 107069 (2020).
- ³⁹M. V. Ivanov, F. H. Bangerter, P. Wójcik, and A. I. Krylov, J. Phys. Chem. Lett. (2020), 10.1021/acs.jpclett.0c01960.
- ⁴⁰M.-S. Xu, C.-L. Yang, M.-S. Wang, X.-G. Ma, and W.-W. Liu, J. Quant. Spectrosc. Radiat. Transf. **242**, 106770 (2020).
- ⁴¹A. L. Collopy, M. T. Hummon, M. Yeo, B. Yan, and J. Ye, New J. Phys. **17**, 55008 (2015).
- ⁴²M. Yeo, M. T. Hummon, A. L. Collopy, B. Yan, B. Hemmerling, E. Chae, J. M. Doyle, and J. Ye, Phys. Rev. Lett. **114**, 223003 (2015).
- ⁴³A. L. Collopy, S. Ding, Y. Wu, I. A. Finneran, L. Anderegg, B. L. Augenbraun, J. M. Doyle, and J. Ye, Phys. Rev. Lett. **121**, 213201 (2018).
- ⁴⁴S. Ding, Y. Wu, I. A. Finneran, J. J. Burau, and J. Ye, Phys. Rev. X **10**, 21049 (2020).
- ⁴⁵C. L. Chalek and J. L. Gole, J. Chem. Phys. **65**, 2845 (1976).
- ⁴⁶K. Liu and J. M. Parson, J. Chem. Phys. **67**, 1814 (1977).
- ⁴⁷C. Linton, J. Mol. Spectrosc. **69**, 351 (1978).
- ⁴⁸A. Bernard and R. Gravina, Astrophysical Journal Supplement Series **52**, 443 (1983).
- ⁴⁹T. C. Steimle and J. E. Shirley, J. Chem. Phys. **92**, 3292 (1990).
- ⁵⁰J. M. Badie and B. Granier, Chem. Phys. Lett. **364**, 550 (2002).
- $^{51}\mathrm{J.-H.}$ Leung, T. Ma, and A. S. C. Cheung, J. Mol. Spectrosc. $\mathbf{229},\,108$ (2005).
- ⁵²D. Zhang, Q. Zhang, B. Zhu, J. Gu, B. Suo, Y. Chen, and D. Zhao, J. Chem. Phys. **146**, 114303 (2017).
- ⁵³J. F. Stanton, J. Gauss, L. Cheng, M. E. Harding, D. A. Matthews, and P. G. Szalay, "CFOUR, Coupled-Cluster techniques for Computational Chemistry, a quantum-chemical program package," With contributions from A.A. Auer, R.J. Bartlett, U. Benedikt, C.

- Berger, D.E. Bernholdt, Y.J. Bomble, O. Christiansen, F. Engel, R. Faber, M. Heckert, O. Heun, M. Hilgenberg, C. Huber, T.-C. Jagau, D. Jonsson, J. Jusélius, T. Kirsch, K. Klein, W.J. Lauderdale, F. Lipparini, T. Metzroth, L.A. Mück, D.P. O'Neill, D.R. Price, E. Prochnow, C. Puzzarini, K. Ruud, F. Schiffmann, W. Schwalbach, C. Simmons, S. Stopkowicz, A. Tajti, J. Vázquez, F. Wang, J.D. Watts and the integral packages MOLECULE (J. Almlöf and P.R. Taylor), PROPS (P.R. Taylor), ABACUS (T. Helgaker, H.J. Aa. Jensen, P. Jørgensen, and J. Olsen), and ECP routines by A. V. Mitin and C. van Wüllen. For the current version, see http://www.cfour.de.
- ⁵⁴D. A. Matthews, L. Cheng, M. E. Harding, F. Lipparini, S. Stopkowicz, T.-C. Jagau, P. G. Szalay, J. Gauss, and J. F. Stanton, J. Chem. Phys. **152**, 214108 (2020).
- ⁵⁵J. F. Stanton, J. Gauss, J. D. Watts, and R. J. Bartlett, J. Chem. Phys. **94**, 4334 (1991).
- ⁵⁶J. D. Watts, J. Gauss, and R. J. Bartlett, J. Chem. Phys. **200**, 1 (1992).
- ⁵⁷L. Cheng and J. Gauss, J. Chem. Phys. **135**, 084114 (2011).
- ⁵⁸D. A. Matthews, J. Gauss, and J. F. Stanton, J. Chem. Theory Comput. 9, 2567 (2013).
- ⁵⁹D. A. Matthews and J. F. Stanton, J. Chem. Phys. **142**, 064108 (2015).
- $^{60}\mathrm{M}.$ Nooijen and R. J. Bartlett, J. Chem. Phys. $\mathbf{102},\,3629$ (1995).
- ⁶¹ J. H. Baraban, D. A. Matthews, and J. F. Stanton, J. Chem. Phys. **144**, 1 (2016).
- $^{62}\mathrm{J}.$ F. Stanton and J. Gauss, J. Chem. Phys. $\mathbf{111},\,8785$ (1999).
- $^{63}{\rm K.~G.~Dyall,~J.~Chem.~Phys.~{\bf 115},~9136~(2001)}.$
- $^{64}\mathrm{W}.$ Liu and D. Peng, J. Chem. Phys. $\boldsymbol{131},$ 1 (2009).
- $^{65}\mathrm{C}.$ Zhang and L. Cheng, Mol. Phys. , e1768313 (2020).
- ⁶⁶K. Klein and J. Gauss, J. Chem. Phys. **129**, 194106 (2008).
- ⁶⁷E. Epifanovsky, K. Klein, S. Stopkowicz, J. Gauss, and A. I. Krylov, J. Chem. Phys. 143, 064102 (2015).

- ⁶⁸L. Cheng, F. Wang, J. Stanton, and J. Gauss, J. Chem. Phys. **148**, 044108 (2018).
- ⁶⁹K. Raghavachari, G. W. Trucks, J. A. Pople, and M. Head-Gordon, Chem. Phys. Lett. 157, 479 (1989).
- ⁷⁰R. J. Bartlett, J. D. Watts, S. A. Kucharski, and J. Noga, Chem. Phys. Lett. **165**, 513 (1990).
- ⁷¹ J. Liu, Y. Shen, A. Asthana, and L. Cheng, J. Chem. Phys. **148**, 034106 (2018).
- ⁷²K. G. Dyall, J. Chem. Phys. **106**, 9618 (1997).
- $^{73}{\rm M}.$ Iliaš and T. Saue, J. Chem. Phys. **126**, 64102 (2007).
- ⁷⁴J. Liu and L. Cheng, J. Chem. Phys. **148**, 144108 (2018).
- ⁷⁵A. T. B. Gilbert, N. A. Besley, and P. M. W. Gill, J. Phys. Chem. A **112**, 13164 (2008).
- ⁷⁶B. O. Roos, R. Lindh, P.-Å. Malmqvist, V. Veryazov, and P.-O. Widmark, J. Phys. Chem. A 109, 6575 (2005).
- ⁷⁷K. A. Peterson, D. Figgen, M. Dolg, and H. Stoll, J. Chem. Phys. **126**, 124101 (2007).
- ⁷⁸D. E. Woon and T. H. Dunning, Jr., J. Chem. Phys. **103**, 4572 (1995).
- ⁷⁹I. M. Mills, in *Molecular Spectroscopy: Modern Research*, edited by K. N. Rao and C. W. Mathews (Academic Press, New York, 1972) pp. 115–140.
- ⁸⁰S. R. Langhoff and C. W. Bauschlicher, J. Chem. Phys. **89**, 2160 (1988).
- ⁸¹T. Helgaker, W. Klopper, H. Koch, and J. Noga, J. Chem. Phys. **106**, 9639 (1997).
- $^{82}{\rm S.}$ Ding, Y. Wu, I. A. Finneran, J. J. Burau, and J. Ye, Phys. Rev. X ${f 10},\,021049$ (2020).
- ⁸³M. A. Norcia, J. R. Cline, J. P. Bartolotta, M. J. Holland, and J. K. Thompson, New Journal of Physics 20, 023021 (2018).
- ⁸⁴J. P. Bartolotta, M. A. Norcia, J. R. Cline, J. K. Thompson, and M. J. Holland, Physical Review A 98, 023404 (2018).

- ⁸⁵S. Snigirev, A. J. Park, A. Heinz, I. Bloch, and S. Blatt, Physical Review A 99, 063421 (2019).
- ⁸⁶J. P. Bartolotta and M. J. Holland, Physical Review A **101**, 053434 (2020).
- ⁸⁷D. DeMille, Phys. Rev. Lett. **88**, 067901 (2002).
- ⁸⁸K.-K. Ni, T. Rosenband, and D. D. Grimes, Chemical science 9, 6830 (2018).
- ⁸⁹S. A. Moses, J. P. Covey, M. T. Miecnikowski, B. Yan, B. Gadway, J. Ye, and D. S. Jin, Science 350, 659 (2015).
- ⁹⁰L. Anderegg, L. W. Cheuk, Y. Bao, S. Burchesky, W. Ketterle, K.-K. Ni, and J. M. Doyle, Science 365, 1156 (2019).
- ⁹¹L. Caldwell and M. Tarbutt, Physical Review Research 2, 013251 (2020).
- ⁹²A. M. Kaufman, B. J. Lester, and C. A. Regal, Phys. Rev. X 2, 041014 (2012).
- ⁹³M. Norcia, A. Young, and A. Kaufman, Phys. Rev. X **8**, 041054 (2018).
- ⁹⁴A. Cooper, J. P. Covey, I. S. Madjarov, S. G. Porsev, M. S. Safronova, and M. Endres, Phys. Rev. X 8, 041055 (2018).
- ⁹⁵S. Saskin, J. Wilson, B. Grinkemeyer, and J. Thompson, Phys. Rev. Lett. 122, 143002 (2019).
- ⁹⁶M. Heckert, M. Kállay, and J. Gauss, Mol. Phys. **103**, 2109 (2005).
- ⁹⁷M. Heckert, M. Kállay, D. P. Tew, W. Klopper, and J. Gauss, J. Chem. Phys. **125**, 044108 (2006).

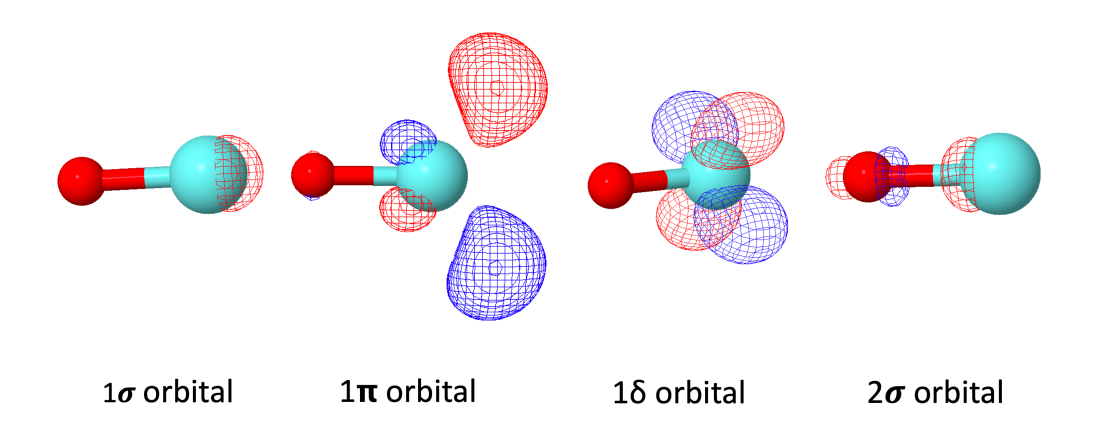


FIG. 2. Frontier molecular orbitals of YO.

TABLE I. The effective Hamiltonian (cm⁻¹) diagonalized to obtain the low-lying spin-orbit-coupled states of YO in the bond length of 1.8 Å. Spin-orbit matrix elements (the off-diagonal elements) have been calculated using the SFX2C-1e EOM-CCSD transition density matrices and the SFX2C-1e AMF spin-orbit integrals, while the scalar-relativistic energies (the diagonal elements) are the SFX2C-1e-CCSD(T)/ ∞ Z values.

	$X^2 \Sigma^+(m_s = \frac{1}{2})$	$A^2\Pi_y(m_s=-\frac{1}{2})$	$A^2\Pi_x(m_s=-\frac{1}{2})$	$A'^2 \Delta_{xy}(m_s = \frac{1}{2}) A$	$A'^2 \Delta_{2z^2 - x^2 - y^2} (m_s = \frac{1}{2})$	$\frac{1}{2}$) B ² $\Sigma^+(m_s = \frac{1}{2})$
$X^2\Sigma^+(m_s=\tfrac{1}{2})$	0	-87.8i	87.8	0	0	0
$A^2\Pi_y(m_s=-\tfrac{1}{2})$	89.1i	16544.7	-203.3i	-27.5	27.5i	-203.7i
$A^2\Pi_x(m_s=-\tfrac{1}{2})$	89.1	203.3i	16544.7	-27.5i	-27.5	-203.7
$A'^2 \Delta_{xy}(m_s = \frac{1}{2})$	0	-26.1	26.1i	14651.2	140.3i	0
$A'^2 \Delta_{2z^2 - x^2 - y^2} (m_s = \frac{1}{2})$	0	-26.1i	-26.1	-140.3i	14651.2	0
$2B^2\Sigma^+(m_s = \frac{1}{2})$	0	206.1i	-206.1	0	0	20999.9

TABLE II. Combination coefficients of scalar-relativistic wavefunctions to compose the spin-orbitcoupled wavefunctions obtained by diagonalizing the effective Hamiltonian in Table I.

	$X^2\Sigma^+$	$A^2\Pi$	$A'^2\Delta$	$B^2\Sigma^+$
$\overline{X^2\Sigma_{1/2}^+}$	0.99997	0.00771	0	0.0001
$A'^2\Delta_{3/2}$	0	0.02454	0.99970	0
$A'^2\Delta_{5/2}$	0	0	1.0	0
$A^2\Pi_{1/2}$	0.00760	0.99803	0	0.06221
$A^2\Pi_{3/2}$	0	0.99973	0.02334	0
$B^2\Sigma_{1/2}^+$	0.00036	0.06150	0	0.99811

TABLE III. SFX2C-1e-EOM-CCSD transition dipole moments (a.u.) between scalar-relativistic wavefunctions as well as the dipole moments of the scalar-relativistic wavefunctions computed at the bond length of 1.8~Å using the TZ basis sets.

	$X^2\Sigma^+$	$A^2\Pi_y$	$A^2\Pi_x$	$A'^2\Delta_{xy}$	$A'^2 \Delta_{2z^2 - x^2 - y^2}$	$B^2\Sigma^+$
$X^2\Sigma^+$	1.87	-2.11	-2.11	0	0	-1.66
$A^2\Pi_y$	-2.10	1.59	0	1.06	-1.06	0.10
$A^2\Pi_x$	-2.10	0	1.59	1.06	1.06	0.10
$A'^2\Delta_{xy}$	0	1.07	1.07	3.07	0	0
$A'^2 \Delta_{2z^2 - x^2 - y^2}$	0	-1.07	1.07	0	3.07	0
$B^2\Sigma^+$	-1.68	0.07	0.07	0	0	0.78

TABLE IV. The square of electronic transition dipole moments, $|\text{TDM}|^2$, and the oscillator strengths for transitions between spin-orbit-coupled wavefunctions computed at the bond length of 1.8 Å. The Einstein A coefficients for the corresponding spontaneous emission are also presented.

	$ TDM ^2$	Oscillator strength	Einstein A coefficient
	(a.u.)	(a.u.)	(s^{-1})
$A^2\Pi_{1/2,\mp 1/2} \to X^2\Sigma^+_{1/2,\pm 1/2}$	4.43	2.19E-01	3.90E + 07
$A^2\Pi_{1/2,\pm 1/2} \to X^2\Sigma^+_{1/2,\pm 1/2}$	0.01	5.14E-04	9.13E + 04
$A^2\Pi_{3/2,\pm 3/2} \to X^2\Sigma^+_{1/2,\pm 1/2}$	4.44	2.26E-01	4.23E + 07
$A'^2\Delta_{3/2,\pm 3/2} \to X^2\Sigma^+_{1/2,\pm 1/2}$	4.0E-03	1.77E-04	2.50E + 04
$B^2\Sigma^+_{1/2,\pm 1/2} \to X^2\Sigma^+_{1/2,\pm 1/2}$	2.76	1.74E-01	5.02E + 07
$B^2\Sigma^+_{1/2,\mp 1/2} \to X^2\Sigma^+_{1/2,\pm 1/2}$	1.7E-02	1.06E-03	3.06E + 05
$A^2\Pi_{1/2,\pm 1/2} \to A'^2\Delta_{3/2,\pm 3/2}$	2.26	1.23E-02	2.61E + 04
$A^2\Pi_{3/2,\pm 3/2} \to A'^2\Delta_{3/2,\pm 3/2}$	1.0E-03	7.16E-06	2.34E + 01
$B^2\Sigma^+_{1/2,\pm 1/2} \to A'^2\Delta_{3/2,\pm 3/2}$	8.2E-03	1.56E-04	4.08E + 03
$A^2\Pi_{3/2,\pm 3/2} \to A'^2\Delta_{5/2,\pm 5/2}$	2.27	1.30E-02	3.04E + 04
$B^2\Sigma^+_{1/2,\pm 1/2} \to A^2\Pi_{1/2,\mp 1/2}$	7.2E-03	9.74 E-05	1.30E + 03
$B^2\Sigma^+_{1/2,\pm 1/2} \to A^2\Pi_{1/2,\pm 1/2}$	2.4E-03	3.22 E-05	4.31E + 02
$B^2\Sigma^+_{1/2,\pm 1/2} \to A^2\Pi_{3/2,\pm 3/2}$	7.6E-03	9.30E-05	1.02E+03

TABLE V. Equilibrium bond lengths (Å) for low-lying electronic states of YO. "lc" and "sc" refer to freezing 15 and 5 core orbitals in coupled-cluster calculations, respectively.

	$X^2\Sigma^+$	$A'^2\Delta \ (^2\Delta_{3/2}/^2\Delta_{5/2})$	$A^2\Pi \ (A^2\Pi_{1/2}/A^2\Pi_{3/2})$	$B^2\Sigma^+$
EOM-CCSD/TZ/lc	1.7813	1.8038	1.7838	1.8125
$\rm EOM\text{-}CCSDT/TZ/lc$	1.7979	1.8261	1.8006	1.8313
CCSD(T)/TZ/lc	1.7922	1.8184	1.7955	1.8262
$\rm EOM\text{-}CCSD/\infty Z/sc\text{+}\Delta T$	1.7909	1.8198	1.7951	1.8252
${\rm EOM\text{-}CCSD}/{\infty}{\rm Z/sc\text{+}}\Delta{\rm T\text{+}}\Delta{\rm SO}$	1.7921	1.8212/1.8205	1.7968/1.7959	1.8263
$\mathrm{SO\text{-}CCSD}(\mathrm{T})/\mathrm{TZ/sc}$	1.7915	1.8180/1.8172	1.7951/1.7943	/
$\mathrm{SO\text{-}CCSD}(\mathrm{T})/\mathrm{QZ/sc}$	1.7883	1.8153/1.8144	1.7928/1.7921	/
$\mathrm{SO\text{-}CCSD}(\mathrm{T})/\infty\mathrm{Z/sc}$	1.7859	1.8123/1.8115	1.7911/1.7904	/
Experiment	1.7875	1.8184	1.7936	1.8252

TABLE VI. Harmonic vibrational frequencies (cm⁻¹) for low-lying electronic states of YO. "lc" and "sc" refer to freezing 15 and 5 core orbitals in coupled-cluster calculations, respectively.

	$X^2\Sigma^+$	$A'^2\Delta \ (^2\Delta_{3/2}/^2\Delta_{5/2})$	$A^2\Pi\ (A^2\Pi_{1/2}/A^2\Pi_{3/2})$	$B^2\Sigma^+$
EOM-CCSD/TZ/lc	893.8	837.1	860.1	817.8
$\rm EOM\text{-}CCSDT/TZ/lc$	851.6	784.9	818.4	775.2
CCSD(T)/TZ/lc	864.2	797.6	829.1	788.3
$\rm EOM\text{-}CCSD/\infty Z/sc\text{+}\Delta T$	853.5	785.7	815.9	774.6
$EOM\text{-}CCSD/\infty Z/sc+\Delta T+\Delta SO$	852.3	784.5/785.4	813.8/814.5	773.1
$\mathrm{SO\text{-}CCSD}(\mathrm{T})/\mathrm{TZ/sc}$	866.0	798.7/799.9	830.7/831.5	/
$\mathrm{SO\text{-}CCSD}(\mathrm{T})/\mathrm{QZ/sc}$	866.0	798.9/800.2	827.9/828.6	/
$\mathrm{SO\text{-}CCSD}(\mathrm{T})/\infty\mathrm{Z/sc}$	866.0	799.1/800.3	826.5/825.9	/
Experiment	862.0	794.6	821.5	758.7/765.5

TABLE VII. Equilibrium term energies (cm⁻¹) for low-lying electronic states of YO. "lc" and "sc" refer to freezing 15 and 5 core orbitals in coupled-cluster calculations, respectively.

	$X^2\Sigma^+$	$A'^2\Delta \ (^2\Delta_{3/2}/^2\Delta_{5/2})$	$A^2\Pi\ (A^2\Pi_{1/2}/A^2\Pi_{3/2})$	$B^2\Sigma^+$
$\rm EOM\text{-}CCSD/TZ/lc$	0	15386.5	16693.8	21620.7
${\rm EOM\text{-}CCSDT/TZ/lc}$	0	14956.5	16706.7	21265.5
CCSD(T)/TZ/lc	0	15149.9	16589.5	21020.4
$\rm EOM\text{-}CCSD/\infty Z/sc\text{+}\Delta T$	0	14486.9	16659.5	21169.6
$\overline{\text{EOM-CCSD}/\infty\text{Z/sc+}\Delta\text{T+}\Delta\text{SO}}$	0	14344.7/14629.8	16441.2/16864.5	21189.4
$\mathrm{SO\text{-}CCSD}(\mathrm{T})/\mathrm{TZ/sc}$	0	15144.5/15469.7	16417.3/16846.6	/
$\mathrm{SO\text{-}CCSD}(\mathrm{T})/\mathrm{QZ/sc}$	0	14766.3/15097.0	16369.4/16802.0	/
$\mathrm{SO\text{-}CCSD}(\mathrm{T})/\infty\mathrm{Z/sc}$	0	14491.0/14825.7	16335.6/16770.5	/
Experiment	0	14531.2/14870.4	16315.8/16746.8	20793.33

TABLE VIII. Variation of calculated FCFs for the $A^2\Pi(0) \to X^2\Sigma^+(\nu)$, $B^2\Sigma^+(0) \to X^2\Sigma^+(\nu)$, and $A'^2\Delta(0) \to X^2\Sigma^+(\nu)$ transitions with respect to the shift of bond-length differences $R_e(A^2\Pi) - R_e(X^2\Sigma^+)$, $R_e(B^2\Sigma^+) - R_e(X^2\Sigma^+)$, and $R_e(A'^2\Delta) - R_e(X^2\Sigma^+)$. The origin refers to the use of EOM-CCSD/ ∞ Z/sc+ Δ T potential energy curves. FCFs greater than 0.001% are explicitly given.

	Shifts of bond-length difference (Å)						
transitions	ν	-0.003	0.000	0.003	0.005	0.010	0.020
$A^2\Pi(0) \to X^2\Sigma(\nu)$	0	99.938%	99.643%	99.049%	98.491%	96.541%	90.459%
	1	0.039%	0.338%	0.928%	1.480%	3.392%	9.181%
	2	0.022%	0.020%	0.023%	0.029%	0.066%	0.353%
	3	<0.001%	<0.001%	<0.001%	<0.001%	0.001%	0.007%
$B^2\Sigma(0) \to X^2\Sigma(\nu)$	0	84.897%	82.195%	79.345%	77.374%	72.244%	61.460%
	1	13.848%	16.127%	18.450%	20.005%	23.842%	30.803%
	2	1.185%	1.575%	2.055%	2.429%	3.571%	6.786%
	3	0.066%	0.098%	0.143%	0.182%	0.322%	0.873%
	4	0.003%	0.004%	0.007%	0.009%	0.020%	0.074%
	5	<0.001%	<0.001%	<0.001%	<0.001%	0.001%	0.004%
$A'^2\Delta(0)\to X^2\Sigma(\nu)$	0	89.306%	86.907%	84.323%	82.508%	77.690%	67.207%
	1	10.058%	12.198%	14.443%	15.981%	19.895%	27.477%
	2	0.612%	0.857%	1.174%	1.432%	2.258%	4.810%
	3	0.023%	0.037%	0.058%	0.077%	0.149%	0.476%
	4	0.001%	0.001%	0.002%	0.003%	0.006%	0.029%
	5	<0.001%	<0.001%	<0.001%	<0.001%	<0.001%	0.001%

TABLE IX. Franck-Condon factors calculated using EOM-CC potential energy curves. In the last column with spin-orbit coupling included, $X^2\Sigma^+$, $B^2\Sigma^+$, $A^2\Pi$, and $A'^2\Delta$ refer to $X^2\Sigma^+_{1/2}$, $B^2\Sigma^+_{1/2}$, $A^2\Pi_{1/2}$, and $A'^2\Delta_{3/2}$, respectively. FCFs greater than 0.001% are explicitly given.

		CCSD/	CCSDT/	CCSD/	CCSD/	CCSD/
transitions	ν	$\mathrm{TZ/lc}$	$\mathrm{TZ/lc}$	$\infty Z/lc + \Delta T$	$\infty Z/sc + \Delta T$	∞ Z/sc+T+ Δ SO
$A^2\Pi(0) \to X^2\Sigma^+(\nu)$	0	99.851%	99.836%	99.600%	99.643%	99.563%
	1	0.135%	0.149%	0.380%	0.338%	0.416%
	2	0.014%	0.015%	0.020%	0.020%	0.020%
$B^2\Sigma^+(0) \to X^2\Sigma^+(\nu)$	0	84.296%	83.034%	81.885%	82.195%	82.411%
	1	14.367%	15.444%	16.372%	16.127%	15.954%
	2	1.262%	1.434%	1.633%	1.575%	1.536%
	3	0.072%	0.085%	0.104%	0.098%	0.094%
	4	0.003%	0.004%	0.005%	0.004%	0.004%
$A'^2\Delta(0) \to X^2\Sigma^+(\nu)$	0	91.389%	87.518%	86.805%	86.907%	86.600%
	1	8.210%	11.661%	12.287%	12.198%	12.464%
	2	0.389%	0.787%	0.869%	0.857%	0.895%
	3	0.011%	0.033%	0.038%	0.037%	0.040%
	4	<0.001%	0.001%	0.001%	0.001%	0.001%

TABLE X. Calculated FCFs for transition using a variety of potential energy curves. "EOM" refers to using ab initio EOM-CCSD/ ∞ Z/sc+ Δ T potential energy curves. "Harmonic (EOM)" and "Morse (EOM)" denote the use of harmonic and Morse potentials with ab initio spectroscopic parameters. "Morse (Exp.)" refers to using a Morse potential with experimental parameters. "EOM (shifted)" refers to the use of the ab initio potential shifted to match the experimental equilibrium bond length. FCFs greater than 0.001% are explicitly given.

transitions	ν	EOM	Harmonic (EOM)	Morse (EOM)	Morse (Exp.)	EOM (shifted)
$A^2\Pi(0) \to X^2\Sigma(\nu)$	0	99.643%	99.679%	99.648%	99.261%	99.301%
	1	0.338%	0.288%	0.333%	0.715%	0.678%
	2	0.020%	0.032%	0.019%	0.024%	0.021%
$B^2\Sigma(0) \to X^2\Sigma(\nu)$	0	82.195%	82.423%	82.142%	76.584%	77.174%
	1	16.127%	15.068%	16.176%	20.345%	20.160%
	2	1.575%	2.204%	1.579%	2.784%	2.469%
	3	0.098%	0.271%	0.098%	0.266%	0.187%
	4	0.004%	0.030%	0.004%	0.020%	0.010%
	5	<0.001%	0.003%	<0.001%	0.001%	<0.001%
$A'^2\Delta(0) \to X^2\Sigma(\nu)$	0	86.907%	87.087%	86.912%	85.018%	85.204%
	1	12.198%	11.472%	12.197%	13.879%	13.685%
	2	0.857%	1.305%	0.853%	1.053%	1.060%
	3	0.037%	0.125%	0.037%	0.049%	0.050%
	4	0.001%	0.011%	0.001%	0.001%	0.002%
	5	<0.001%	0.001%	<0.001%	<0.001%	<0.001%